NANO LETTERS

2008
Vol. 8, No. 2
737−742

Arrays of Iso-Oriented Gold Nanobelts

Ying Chen, Srdjan Milenkovic, and Achim Walter Hassel*

Max-Planck-Institut für Eisenforschung GmbH, Max-Planck Str. 1, D-40237 Düsseldorf, Germany

Received October 7, 2007; Revised Manuscript Received December 16, 2007

ABSTRACT

For the first time single crystalline gold nanobelt arrays with identical crystallographic orientation were obtained. A combined method consisting of directional solid-state transformation of a Fe–Au eutectoid and a well controlled electrochemical treatment enables production of arrays of nanobelts with a desired length. They have an average thickness of 25 nm and width of 200–250 nm, respectively. The obtained gold nanobelt arrays were characterized by electron backscattered diffraction (EBSD), X-ray diffraction, and XPS. The underlying mechanisms and the potential of this method for the production of nanosensors are discussed.

Intensive approaches have been devoted to the systematic control of the crystal shapes and arrays of metal nanomaterials, for their applications in physics and for the fabrication of nanodevices.[1−3] The intrinsic properties of metal nanostructures can be tuned by controlling size, shape, arrangement, and crystallinity.[4−5] One-dimensional metallic nanostructures, such as nanowires, nanorods, and nanobelts (nanoribbons), have attracted significant research interest taking advantage of their promising mechanical, electronic, optical, and other properties with respect to dimensionality and size confinement.[6−7] Nanobelts, especially nanobelts composed of semiconductors, have been extensively studied because they may represent a good system for examining dimensionally confined transport phenomena and for fabricating functional nanodevices based on individual nanobelts.[8] There are many reports about the preparation of oxides[8−10] and sulfides;[11−12] however, the report on the synthesis of metal nanobelts, especially noble metal nanobelts, is rarely seen. The only known examples are the preparation of Ag nanobelts by refluxing an aqueous silver colloidal dispersion[13] or by reduction of $AgNO_3$ with ascorbic acid in the presence of poly(acrylic acid) (PAA);[14] the growth of Cu nanobelts on the surface of an Al TEM grid by galvanic reduction;[15] and the growth of Ni nanobelts through a hydrothermal method.[16] Very recently, Han et al. reported on the synthesis of gold nanobelts dispersed in solution by reduction of $HAuCl_4$ with α-D-glucose under sonification;[17] and Zhang et al. prepared gold nanobelts via one-dimensional self-assembly of triangular Au nanoplates.[18]

Nanoarrays on a surface have a potential for applications in optoelectronics, information storage, and electrochemical sensing.[19] For example, when gold nanowires are organized in an array, the resulting electrodes could combine the advantages of both, that of a nanoelectrode and the signal intensity from a macroscopic electrode. Among various fabrication methods of nanoarrays, the so-called "template" method, named by C. R. Martin,[20] especially a "hard" template such as Anodized Aluminum Oxide (AAO), was extensively studied due to its controllable effect on product size and shape through the template structure. Therefore, this template method has been widely used to prepare nanostructures with various morphologies such as nanowires, nanotubes, nanowells, nanopillars, and even nanobarcodes composed of different metals or a combination of metal and semiconductor.[19−25] For the preparation of gold nanowires, Sander[19] produced gold nanodot arrays by evaporation and gold nanorod arrays by electrochemical deposition; Wirtz[21] used electrochemical deposition into the AAO template to fabricate gold nanowire and nanotube arrays to form gold nanoelectrodes; Forrer[26] used the same method to form gold nanowire arrays. However, these nanowires are usually polycrystalline, which is often a drawback for their applications. Only in a few cases the wires show a high degree of crystallinity[27−28] but no crystallographic orientation relationship among the wires. The drawback can be, for example, a quantitative description of spectroscopic properties of gold nanowires cannot be achieved, because of the different adsorption abilities for molecules on different crystallographic surfaces.[29] So, it is quite interesting but also challenging to fabricate one-dimensional gold nanostructure arrays, which can find practical applications in nanodevices.[30] Here, it is reported on a method for synthesizing single-crystalline gold nanobelt arrays, embedded in an iron matrix, through directional solidification of an Fe−Au eutectoid alloy. Directional solidification of a eutectic/eutectoid alloy is a method that can facilitate the nanostructuring of a material. It includes directional decomposition of the Fe−Au eutectoid alloy, followed by a phase separation

* Corresponding author. E-mail: hassel@elchem.de. Fax: +49 211 6792 218.

10.1021/nl0725852 CCC: $40.75
Published on Web 02/13/2008

through selective and partial etching of the Fe matrix to release gold nanobelts from the matrix.

This method has several advantages. It produces single crystalline nanobelt arrays embedded in a single crystalline matrix. These gold nanobelts have identical crystallographic orientations even azimuthally in one grain. Nanobelt size and spacing show a narrow distribution and can be controlled by the processing parameters.[31] The spacing between each nanobelt is large enough to study the properties of a single nanobelt. To the best of the authors' knowledge, this is the first example of monocrystalline iso-oriented Au nanobelt arrays reported up to date.

In a previous study, it was confirmed that the eutectoid transformation occurs at 2.3 at. % Au,[32] which agreed well with existing calculated and DTA data.[33] Pre-alloys were prepared using 99.999% Au and 5 times zone melting refined Fe, by induction melting under an Ar atmosphere and drop casting into a cylindrical copper mould. After subsequent fitting into alumina crucibles, samples were directionally transformed in a Bridgman type solidification furnace with resistance heating. The details were described elsewhere.[32] Further, the eutectoid alloy was cut in $1 \times 1 \times 0.1$ cm^3 pieces and ground for further treatment. The selective and partial dissolution of the α-Fe phase in the eutectoid alloy was achieved through electrochemical etching by anodic dissolution. The electrolyte was only slightly different from that for electrochemical polishing for pure iron and was composed of 20 mL of $HClO_4$ and 180 mL of 2-butoxyethanol; the nonaqueous electrolyte was used in order to avoid the hydrolysis of Fe ions. All electrochemical etching experiments were performed at 0 °C to reduce the possible oxidation of ferrous ions. The applied potential varied from 1.5 to 8.0 V (vs counter electrode), and the time of etching was varied between 1 and 30 min. After this procedure, the sample was washed with ethanol, dried, and stored in a desiccator for future characterization.

In order to obtain gold nanobelt arrays with a smooth matrix surface, high potentials were applied to accelerate the etching process, meanwhile, to avoid the local corrosion of iron. After the etching at 5 V (vs counter electrode) for 5 min, arrays of short gold nanobelts were obtained, as shown in Figure 1. Figure 1a and b show the representative field emission scanning electron microscopy images (FE-SEM, LEO 1550VP, GEMINI) of the as-prepared "short" gold nanobelt arrays. Figure 1c shows the high-resolution FE-SEM image of these gold nanobelt arrays. The size of the nanobelts was determined from the SEM images. They have an average thickness of 25 nm, a width of 200−250 nm, and an exposed length of less than 200 nm.

The crystallinity and crystallographic orientation of the obtained gold nanobelt arrays were characterized using an electron backscattering diffraction technique (EBSD, TSL/EDAX, DigiView 1612 camera). To determine the crystallinity and the crystallographic orientation relationship of the gold nanobelts, some gold nanobelts were randomly chosen. First, the short gold nanobelts were cut along the matrix surface with a focused ion beam (FIB, Zeiss XB 1560, equipped with a field emission electron column and a

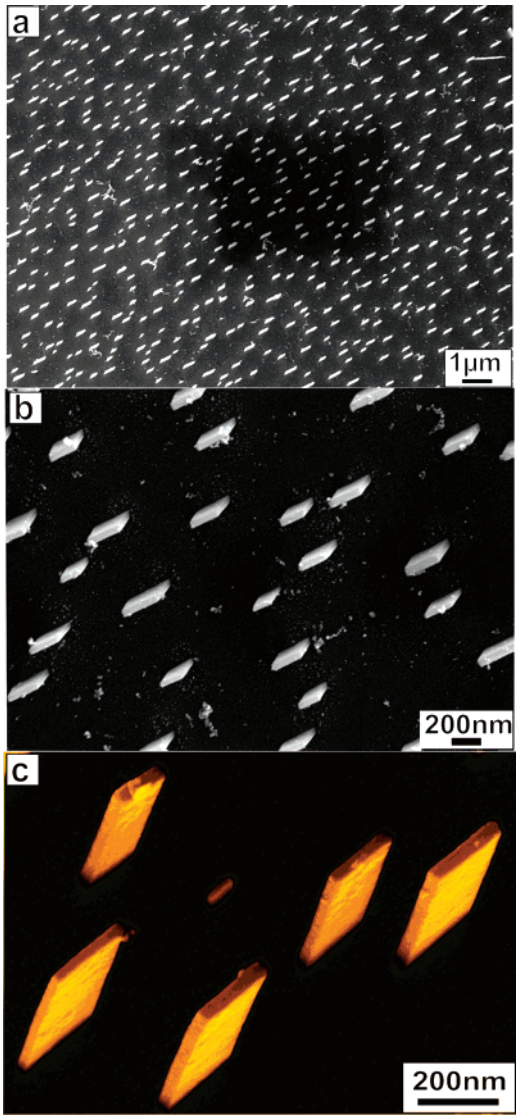

Figure 1. (a, b) FE-SEM images and (c) high-magnification SEM image of as-prepared Au nanobelt arrays; potential $E = 5$ V, etching time $t = 5$ min.

Gallium ion emitter) to get a smooth surface, which is vital for EBSD. The high-quality Kikuchi patterns were clearly observed as shown in Figure 2, and by indexing them, the corresponding Euler angles ($\varphi 1$, Φ, $\varphi 2$) were obtained. Figure 2 shows the Kikuchi patterns of two randomly selected gold nanobelts (a and b) and two different spots of the matrix (c and d), respectively. The results demonstrate that both, the matrix and the belts are single crystalline. Moreover, in one grain, not only the matrix iron has identical crystallographic orientation at different randomly chosen spots but also the different gold nanobelts have the same crystallographic orientation, even azimuthally. This means that the obtained arrays consist of iso-oriented single crystalline gold nanobelts. It should be pointed out that, because it is very difficult to find the exact position where gold nanobelts are perpendicular to the surface, the obtained crystallographic orientations of gold nanobelts may be not exactly the growth direction of the nanobelts. This is part of an ongoing project, and the new result will be reported.

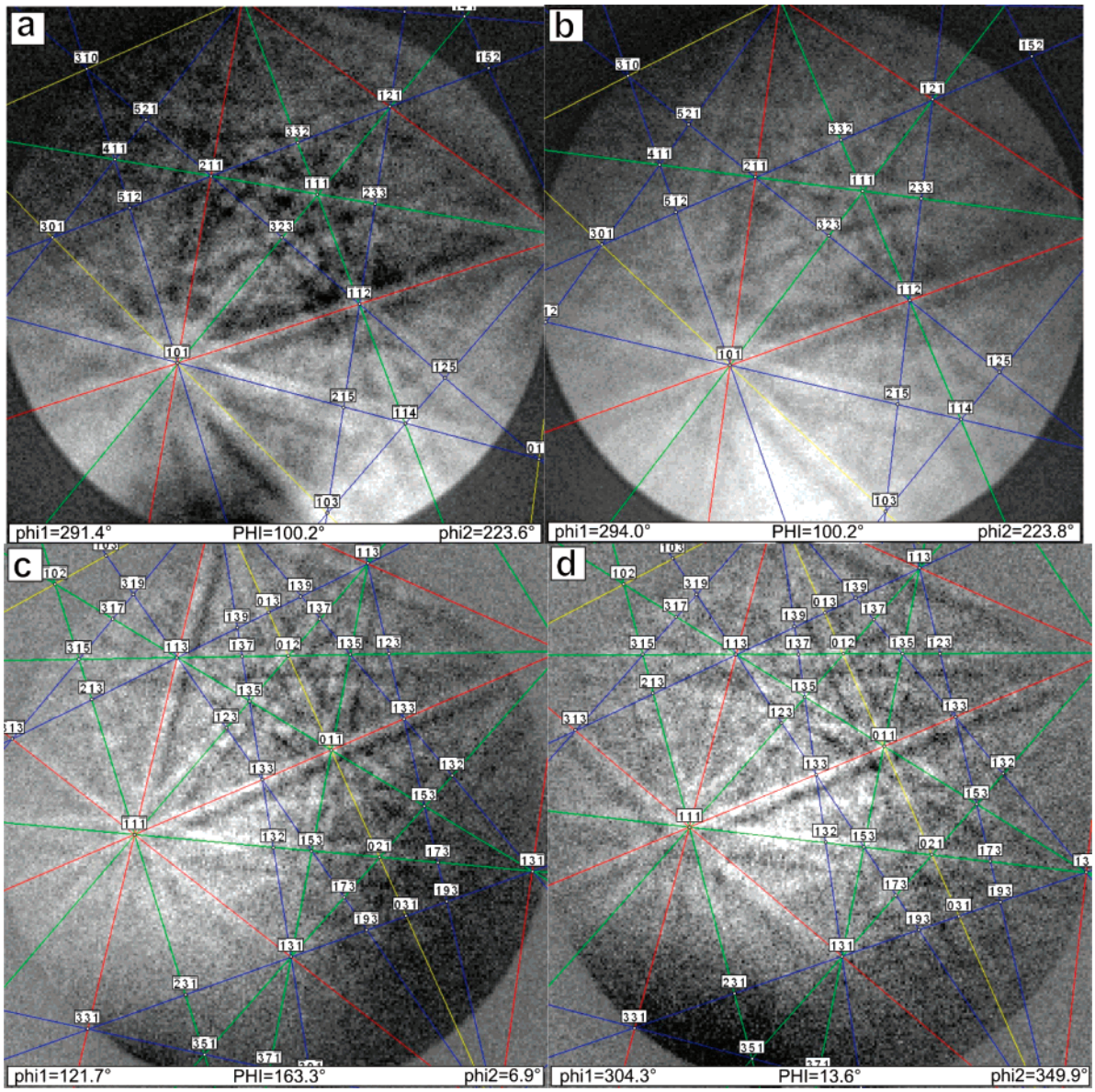

Figure 2. EBSD patterns of Au (a and b) and Fe (c and d) in one sample, which proved that gold nanobelts have the same crystallographic orientation.

X-ray diffraction (XRD, BRUKER axs, D8 X-ray diffractometer) gives further support of the phase structure of the obtained gold nanobelt arrays. Curves in Figure 3 a and b show the diffraction patterns for gold nanobelt arrays before and after partial etching. As shown in Figure 3b, the peaks located at $2\theta = 38.184°$, $2\theta = 44.392°$, and $2\theta = 64.576°$ correspond to the (111), (200), and (220) lattice planes of the face-centered cubic (fcc) structure of gold (JCPDS, File No. 4-0784). Moreover, from Figure 3a, which is the XRD of the sample prior to etching, the difference compared to that of the partially etched sample (Figure 3b) can be clearly seen. The peaks located at $2\theta = 44.673°$ and $2\theta = 65.021°$ correspond to the (110) and (200) lattice planes of body-centered cubic (bcc) α-iron (JCPDE, File No. 6-0696). The peak of (200) of gold is very near to the peak of (110) of α-iron (0.281° difference), and the peak of (220) of gold is also quite near to the peak of (200) of α-iron (0.445° difference); therefore it is difficult to deconvolute the peaks located at 2θ of 44.5° and 64.5°. For the fcc gold, the strongest peak is located at $2\theta = 38.184°$, and for α-iron it is at $2\theta = 44.673°$, so the peak intensity at $2\theta = 38.184°$, $2\theta = 44.5°$, and $2\theta = 64.5°$ can be calculated by multiplying the individual peak intensity with the alloy composition. The result is shown in Table 1. The experimental results of the nonetched sample are quite similar to the calculated results, whereas, for the partially etched sample, the peak located at about $2\theta = 38.184°$ is much stronger than the calculated one. This is clear proof that gold nanobelts of identical orientation are released through this etching process. The gold nanobelt arrays were additionally characterized by X-ray photoelectron spectroscopy (XPS, Physical Electronics Quantum 2000 Scanning ESCA Microprobe, sputtering 2 keV Ar^+). The XPS results (Figure 4) show that the gold nanobelts are pure metallic gold, which can be confirmed from the binding energy for Au $4f_{7/2}$ located at 84 eV, and that the matrix is covered with a thin layer of iron oxide

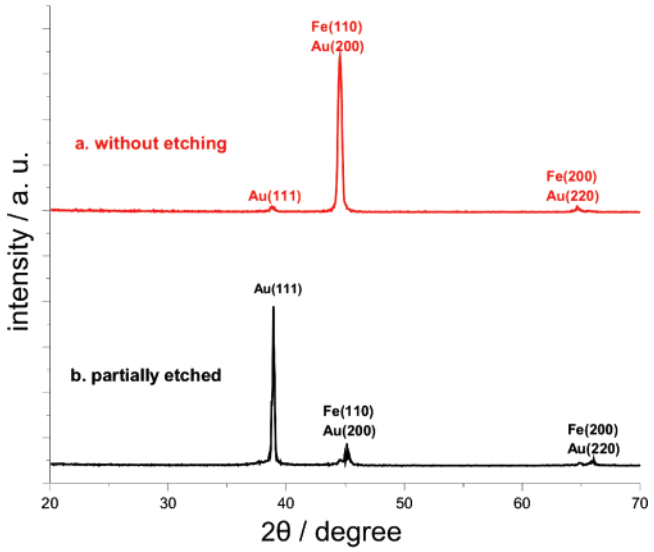

Figure 3. XRD patterns of the unetched (a) and partially etched (b) samples.

Table 1. Theoretical and Experimental Results of XRD Peak Intensity

	$2\theta = 38°$	$2\theta = 44.5°$	$2\theta = 64.5°$
Fe	–	5.0	1.0
Au	3.125	1.625	1.0
$Fe_{97.7}Au_{2.3}$ (theoretical)	1.0	42.998	8.816
$Fe_{97.7}Au_{2.3}$ (experiment)	1.0	34.598	1.189
partially etched	24.543	3.457	1.0

(binding energy for Fe $2p_{3/2}$ is 710 eV) due to the environmental oxidation of pure iron in air. After removal of 5 nm by sputtering, the binding energy for Fe $2p_{3/2}$ shifted to 707 eV (Figure 4b), which coincides with that of Fe^0. The above results proved that the oxide layer is only a few nanometers thick.

Regarding the nanobelt arrays, the length of the nanobelts is of vital importance for their properties. For example, the length of the nanobelts will influence the surface enhanced Raman scattering (SERS) properties, since the different lengths will lead to different surface roughnesses, which is the key factor for SERS.[34] Another example is the electrochemical catalytic property of the nanobelt array electrode. Different lengths of nanobelts will lead to different electrode surface areas, which will in turn dramatically change the electrochemical properties.[34−35] Thus, the length control of the gold nanobelt arrays is of key significance for future applications. In this study, the length of the obtained gold nanobelts was carefully controlled by monitoring the parameters of the electrochemical dissolution process. The potential was varied between 1.5 and 8 V by using a two-electrode system. In order to obtain gold nanobelts with identical lengths in a smooth matrix surface, a local corrosion had to be avoided, which was achieved by increasing the potential or prolonging the etching time. Adjusting these two parameters led to an even dissolution of the surface and to the intended length of nanobelts. At a high potential, the surface was etched away quickly and evenly, but at the same time, the gold was also attacked to some extent. Under this

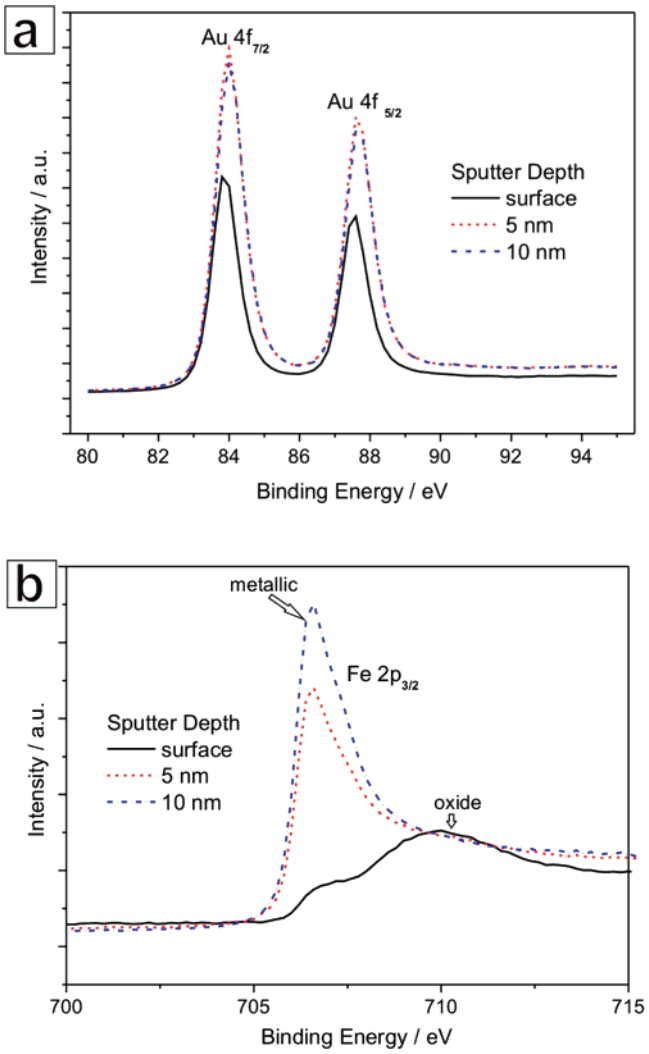

Figure 4. XPS of Au nanobelts (a) and iron matrix (b) in a partially etched sample.

condition, only the short gold nanobelt arrays could be obtained, which can be seen in Figures 1 and 5a. In order to increase the released length of the nanobelts, the applied potential was decreased to reduce the possibility of anodic dissolution of gold and, at the same time, to obtain a smooth matrix surface without local matrix attack, the etching time increased sufficiently to dissolve the entire surface. Figure 5 shows SEM images of the gold nanobelt arrays obtained under various conditions. From Figure 5a to f, the applied potential was reduced from 5 to 1.5 V, meanwhile the etching time was increased from 8 to 30 min. Thus, the length of the gold nanobelt arrays could be controlled from less than 200 nm to dozens of micrometers. Considering that the thickness of the nanobelts is only about 20 nm, the aspect ratio can reach more than 2000! Of course, since the nanobelts are very thin and gold is very soft, nanobelts longer than 5 μm are always lying down, as it can be seen from Figure 5 e and f. Due to the reactivity of pure iron, some iron oxide occasionally appears on the surface of gold nanobelts and on the matrix (see Supporting Information).

The strict control of the electrochemical reaction allows also an intentional local attack of the matrix. When the Fe−

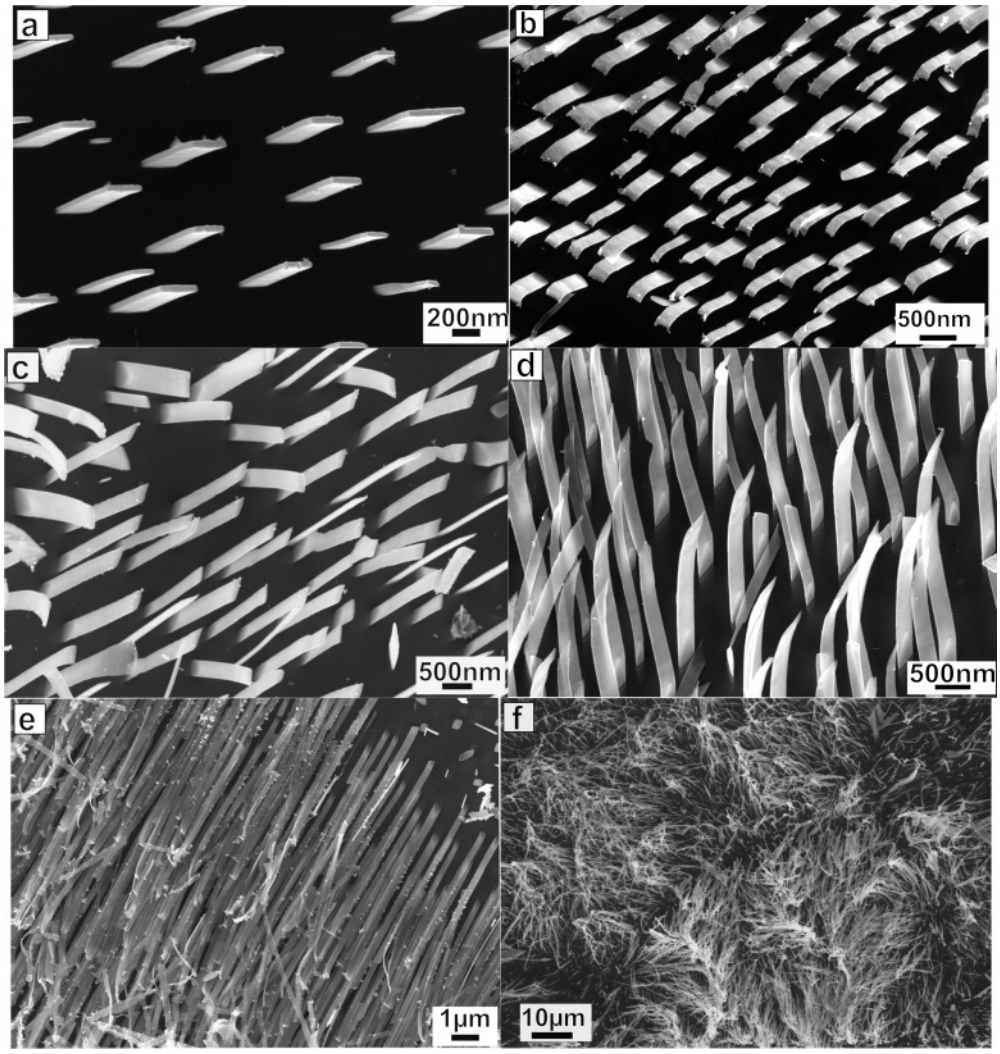

Figure 5. SEM images of nanobelt arrays with different lengths (a) 250 nm, (b) 500 nm, (c) 1 μm, (d) 2 μm, (e) 10 μm, and (f) 30 μm.

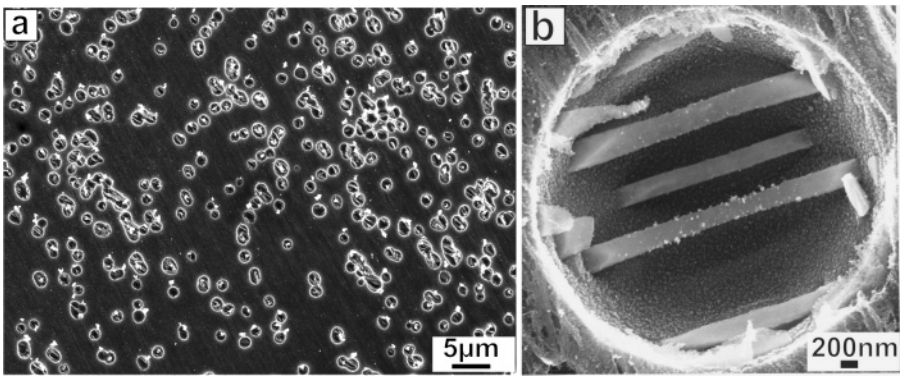

Figure 6. SEM images of general view (a) and a typical pitting hole of the sample in which gold nanobelts are parallel to the surface (b).

Au eutectoid alloy sample was cut along the growth direction (along the axis of the cylinder ingot), the gold nanobelts are embedded in the matrix parallel to the surface. The SEM images shown in Figure 6, which were taken from a longitudinally cut sample anodized at a low potential for a short time (5 V, 1 min), confirm the abovementioned prediction. The gold nanobelts can be clearly seen embedded inside of the matrix and parallel to the surface. Similar features were observed in the NiAl−Re eutectic system, when the sample was anisotropically etched parallel to the growth direction.[36] In that case Re nanowires were stretching through the pits parallel to the sample surface. This kind of "bridging" nanostructures could be employed in the mechanical testing of nanowires or nanobelts.

In summary, for the first time, gold nanoarrays of single crystalline gold nanobelts with long-range identical crystallographic orientation were obtained. Directional solid-state transformation of an Fe−Au eutectoid followed by a

precisely controllable electrochemical treatment enabled the production of arrays with iso-oriented nanobelts of a desired length. The method is simple, convenient, economical, and easily applicable on a large scale. These unique properties allow a quantitative study of the spectroscopic properties as a function of the electrochemical potential and crystallographic orientation. Moreover, the obtained gold nanobelt arrays can later be used as nanosensors and/or nanoelectrodes after appropriate insulation of the interspace left after dissolution of the matrix.

Acknowledgment. Ying Chen acknowledges IMPRS Surmat for financial support through a fellowship. The financial support of the Deutsche-Forschungs-Gemeinschaft through the project Application of Directionally Solidified Nanowire Arrays within the DFG Priority Programme 1165 Nanowires and Nanotubes - From Controlled Synthesis to Function is gratefully acknowledged. Dedicated to Prof. Dieter M Kolb on the occasion of his 65th birthday.

Supporting Information Available: Detailed descriptions of materials and methods, as well as additional figures. This material is available free of charge via the Internet at http://pubs.acs.org.

References

(1) Wang, Z. L. *J. Phys. Chem. B* **2000**, *104*, 1153.
(2) Murphy, C. J. *Science* **2002**, *298*, 2139.
(3) Narayana, R.; El-Sayed, M. A. *Nano Lett.* **2004**, *4*, 1343.
(4) Jin, R.; Cao, Y.; Kelly, C. A.; Schatz, G. C.; Zheng, J. G. *Science* **2001**, *294*, 1901.
(5) El-Sayed, M. A. *Acc. Chem. Res.* **2001**, *34*, 257.
(6) Chen, J.; Wiley, B. J.; Xia, Y. *Langmuir* **2007**, *23*, 4120.
(7) Murphy, C. J.; Sau, T. K.; Gole, A. M.; Orendorff, C. J.; Gao, J.; Gou, L.; Hunyadi, S. E.; Li, T. *J. Phys. Chem. B* **2005**, *109*, 13857.
(8) Pan, Z. W.; Dai, Z. R.; Wang, Z. L. *Science* **2001**, *291*, 1947.
(9) Wen, X.; Wang, S.; Ding, Y.; Wang, Z. L.; Yang, S. *J. Phys. Chem. B* **2005**, *109*, 215.
(10) Ma, R.; Bando, Y.; Zhang, L.; Sasaki, T. *Adv. Mater.* **2004**, *16*, 918.
(11) Yao, W. T.; Yu, S. H.; Pan, L.; Li, J.; Wu, Q. S.; Zhang, L.; Jiang, J. *Small* **2005**, *1*, 320.
(12) Zhu, Y. C.; Bando, Y.; Xue, D. F. *Appl. Phys. Lett.* **2003**, *82*, 1769.
(13) Bai, J.; Qin, Y.; Jiang, C.; Qi, L. *Chem. Mater.* **2007**, *19*, 3367.
(14) Sun, Y.; Mayers, B.; Xia, Y. *Nano Lett.* **2003**, *3*, 675.
(15) Huang, T. K.; Cheng, T. H.; Yen, M. Y.; Hsiao, W. H.; Wang, L. S.; Chen, F. R.; Kai, J. J.; Lee, C. Y.; Chiu, H. T. *Langmuir* **2007**, *23*, 5722.
(16) Liu, Z.; Li, S.; Yang, Y.; Peng, S.; Hu, Z.; Qian, Y. *Adv. Mater.* **2003**, *15*, 1946.
(17) Zhang, J.; Du, J.; Han, B.; Liu, Z.; Jiang, T.; Zhang, Z. *Angew. Chem., Int. Ed.* **2006**, *45*, 1116.
(18) Zhang, J.; Liu, H.; Wang, Z.; Ming, N. *Appl. Phys. Lett.* **2007**, *91*, 133112.
(19) Sander, M. S.; Tan, L. S. *Adv. Funct. Mater.* **2003**, *13*, 393.
(20) Martin, C. R. *Science* **1994**, *266*, 1981.
(21) Wirtz, M.; Martin, C. R. *Adv. Mater.* **2003**, *15*, 445.
(22) Evans, U.; Colavita, P. E.; Doescher, M. S.; Schiza, M.; Myrick, M. L. *Nano Lett.* **2002**, *2*, 641.
(23) Yuan, J.; Wang, K.; Xia, X. *Adv. Funct. Mater.* **2005**, *15*, 803.
(24) Nicewarner-Pena, S. R.; Freeman, R. G.; Reiss, B. D.; He, L.; Pena, D. J.; Walton, I. D.; Cromer, R.; Keating, C. D.; Natan, M. J. *Science* **2001**, *294*, 137.
(25) Lee, J. H.; Wu, J. H.; Liu, H. L.; Cho, J. U.; Cho, M. K.; An, B. H.; Min, J. H.; Noh, S. J.; Kim, Y. K. *Angew. Chem., Int. Ed.* **2007**, *46*, 3663.
(26) Forrer, P.; Schlottig, F.; Siegenthaler, H.; Textor, M. *J. Appl. Electrochem.* **2000**, *30*, 533.
(27) Karim, S.; Toimil-Molares, M. E.; Maurer, F.; Miehe, G.; Ensinger, W.; Liu, J.; Cornelius, T. W.; Neumann, R. *Appl. Phys. A.* **2006**, *84*, 403.
(28) Tian, M.; Wang, J.; Kurtz, J.; Mallouk, T. E.; Chan, M. H. W. *Nano Lett.* **2003**, *3*, 919.
(29) Kamat, P. V. *J. Phys. Chem. B* **2002**, *106*, 7729.
(30) Hassel, A. W.; Smith, A. J.; Milenkovic, S. *Electrochim. Acta* **2006**, *52*, 1799.
(31) Milenkovic, S.; Hassel, A. W.; Schneider, A. *Nano Lett.* **2006**, *6*, 794.
(32) Milenkovic, S.; Schneider, A.; Hassel, A. W. *Gold Bull.* **2006**, *39*, 185.
(33) Isaac, E.; Walter, P. *Z. Anorg. Metallkd.* **1950**, *41*, 234.
(34) Tian, Z. Q.; Ren, B.; Wu, D. Y. *J. Phys. Chem. B* **2002**, *106*, 9463.
(35) Gao, F. F.; El-Deab, M. S.; Okajima, T.; Ohsaka, T. *J. Electrochem. Soc.* **2005**, A1226.
(36) Hassel, A. W.; Bello-Rodriguez, B.; Milenkovic, S. *Electrochim. Acta* **2005**, *51*, 795.

NL0725852